

AIR-SIDE HEAT TRANSFER AND PRESSURE DROP IN TUBE-FIN ACCELERATED FLOW HEAT EXCHANGERS

Paulo J Waltrich
Joel Boeng
Daniel S Vieira
Christian J L Hermes
Cláudio Melo
Jader R Barbosa Jr.

POLO – Research Laboratories for Emerging Technologies in Cooling and Thermophysics
Department of Mechanical Engineering, Federal University of Santa Catarina
Florianópolis, SC, 88040900, Brazil
jrb@polo.ufsc.br

Rodrigo Kremer
Whirlpool Corporation
CIT – Corporate Innovation and Technology
Joinville, SC, Brazil

Abstract. *An experimental analysis of heat transfer and pressure drop on the air-side of tube-fin evaporators utilized in household ‘frost-free’ refrigerators is carried out in the present paper. The performance of an alternative evaporator concept, the so-called Accelerated Flow Evaporator (AFE) is systematically investigated for the first time. In this evaporator, the air-side cross sectional area decreases with the distance from the air flow inlet causing the air flow to accelerate and promote an enhancement of the air-side heat transfer coefficient. This heat transfer enhancement allows a reduction of the heat exchanger volume and hence its material cost. Comparisons between the experimental results and Computational Fluid Dynamics (CFD) simulations are also presented, with the purpose of validating a numerical methodology to be used as a design tool for this new type of evaporator.*

Keywords: *Accelerated flow evaporator, heat exchangers, heat transfer enhancement.*

1. INTRODUCTION

There are more than 10^9 domestic refrigerators currently in operation worldwide (Coulomb, 2006) and the so-called ‘no-frost’ (or ‘frost-free’) refrigerators represent a substantial and increasing fraction of this number. The main difference between a conventional (or ‘static’) and a ‘no-frost’ refrigerator is the type of evaporator used and the associated mode of air flow circulation. In ‘no-frost’ refrigerators, compartment cooling relies on forced convection heat transfer between the internal air (assisted by a fan) and a tube-fin evaporator (Figure 1). In conventional refrigerators, vertical plate evaporators (or ‘roll-bond’ evaporators) are used and air internal circulation is due to natural convection.

The evaporator has an important role in determining the system performance because it affects the size of the freezer and refrigerated compartments and, more importantly, it is responsible for providing the cooling capacity required for preserving the goods stored in the refrigerator. Hence, improving the performance of the evaporator is potentially significant as a means of improving the performance of the whole system and, consequently, as a means of reducing the consumption of electricity and promoting material cost savings.

Cur and Anselmino (1992) proposed an alternative configuration of tube-fin evaporator for ‘no-frost’ domestic appliances, the *Accelerated Flow Evaporator* (AFE). The main purpose of this configuration is to reduce the size of the evaporator (and hence the volume of aluminium) by enhancing the local air-side heat transfer coefficient. This local intensification is achieved through a progressive (linear) reduction of the air-side cross-sectional area, which results in an increase of the mean velocity of the air stream and hence the local Reynolds number. The main drawback of the AFE configuration is an intrinsic increase of the reversible and irreversible components of the pressure drop on the air-side. So far, as far as the open literature is concerned, there has been no systematic study of this type of evaporator and the real benefits of its volumetric reduction and associated increase in air-side pressure drop in comparison with the standard ‘no-frost’ evaporator are yet to be fully quantified.

Even for conventional ‘no-frost’ evaporators, there is a dearth in the open literature regarding systematic studies of their thermal-hydraulic performance. Karatas *et al.* (2000) carried out an experimental study of the air-side heat transfer and pressure drop in ‘no-frost’ evaporators. They tested four evaporators and assessed the effect of non-uniformities in the temperature and velocity distributions of the inlet air flow. Although the number of fins (and hence the fin spacing and finning factor) was different for each evaporator, their basic characteristics such as the longitudinal tube pitch, the transversal tube pitch, the number of tube per row and the face dimensions were kept approximately constant. Karatas *et*

al. (2000) concluded that the heat transfer correlation was equally valid for the non-uniform flow cases if mass flow averaged values of temperature and velocity were used at the evaporator inlet.

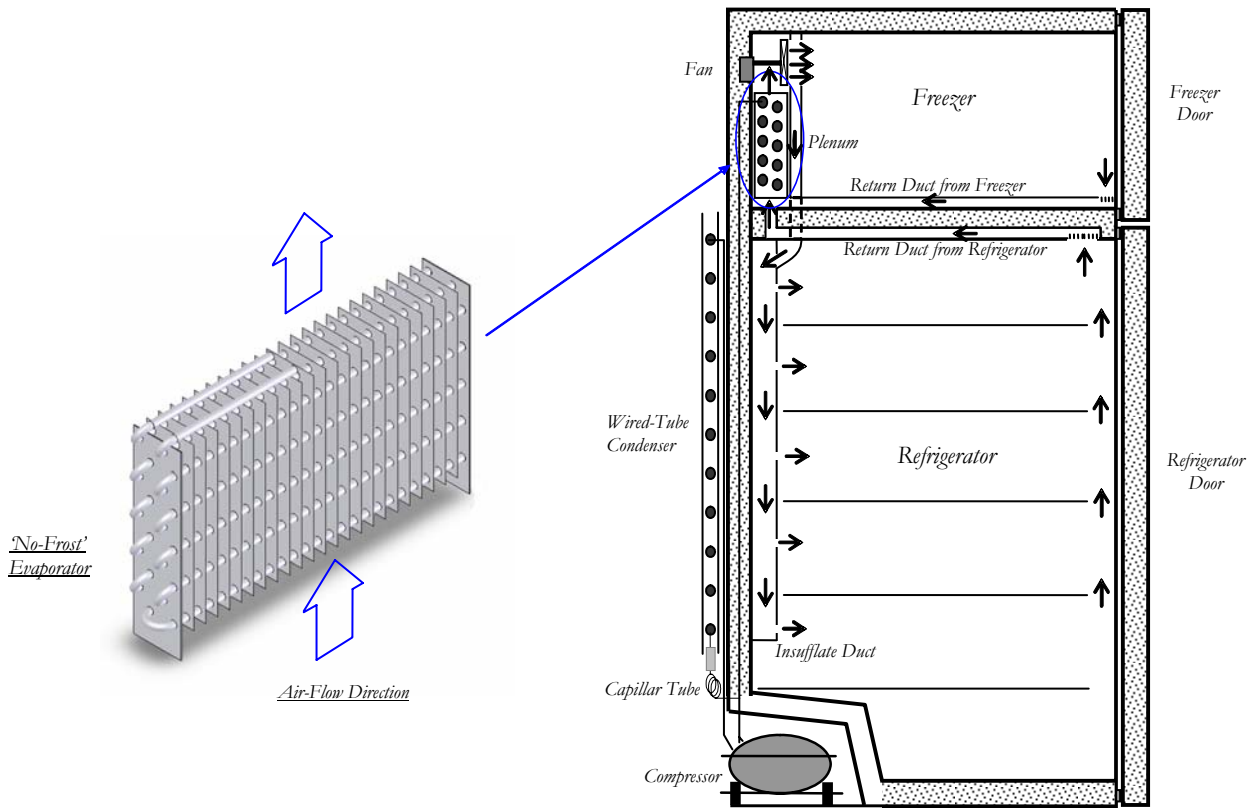


Figure 1. Standard evaporator and side view of a 'No-Frost' refrigerator.

Lee *et al.* (2002) investigated experimentally the behaviour of the air-side heat transfer coefficient for three different evaporator configurations (discrete flat plate fins, continuous flat plate fins and spine fins). Despite its lower length and smaller heat transfer area, the spine finned tube evaporator exhibited the best thermal-hydraulic performance under 'dry' conditions. The range of validity of the correlations proposed by the authors was not indicated and detailed pressure drop were not provided for the three evaporator types investigated by Lee *et al.* (2002). Nevertheless, it was mentioned that the pressure drop of the spine finned evaporator was significantly lower than those of discrete and continuous flat plate fin evaporator.

Melo *et al.* (2004) carried out *in-situ* tests in an actual refrigerator maintaining all of the original characteristics of the air distribution system. Three evaporators with nearly identical geometrical characteristics, but with distinct flow arrangements (parallel-flow, counter-flow and standard, i.e., 2-pass) were evaluated. As expected, the flow arrangement did not show any effect on the heat transfer performance for refrigerant outlet superheat lower than 5°C. However, the counter-flow evaporator exhibited the highest performance at 10°C superheat.

The objective of this paper is to present a systematic study of the influence of two geometric parameters (e.g., number of fins and outlet height) and air flow rate on the air-side thermal-hydraulic performance of a new type of evaporator under 'dry' conditions (no condensate or frost formation). In addition to the experimental work, CFD simulations were carried out to assess and validate the use of such tool in further improvements of the design of AFE's.

2. EXPERIMENTS

2.1. Evaporator Samples

Four evaporator samples made from copper (tubes) and aluminium (fins) were tested. The inner and outer diameters of the tubes in all evaporators are 7.80 and 8.80 mm, respectively. A staggered tube array is used. The fins are flat, plain and continuous. Figure 2 shows a side view of the evaporator samples illustrating the cross-sectional area reduction in the direction of the flow. The width W , the inlet height (thickness) H_{in} and the fin thickness in all samples are 310 mm, 192 mm and 0.25 mm, respectively. The evaporator outlet height (H_{out}), number of fins, the total surface area of fins and tubes, the fin spacing and the amount of material (evaporator mass) are different for each individual sample and their values are summarized in Table 1.

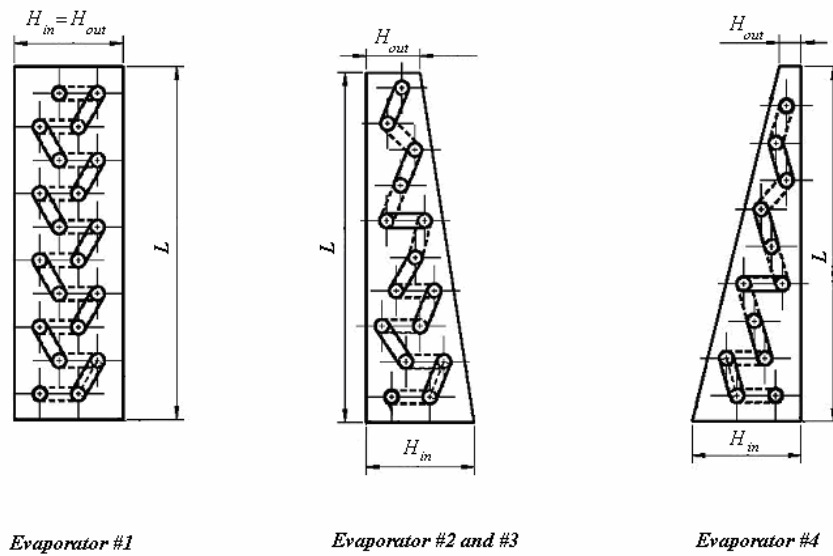






Figure 2. Geometry of the evaporator samples (side view).

Table 1. Geometric parameters of evaporator samples.

Sample N°	H _{out} (mm)	N° of fins	N° of tubes	Surface area (m ²)	Fin pitch (mm)	Mass (kg)
 Sample #1	59.5	60	20	1.41	5.15	1.242
 Sample #2	29.75	30	15	0.60	10.30	0.844
 Sample #3	29.75	60	15	1.07	5.15	0.887
 Sample #4	11.9	57	12	0.80	5.50	0.734

2.2. Experimental Apparatus

An open-loop wind tunnel was designed according to ANSI/ASHRAE Standards 37 (1988), 41.2 (1987) and 51 (1999). The facility was constructed from a double layer of ordinary steel plates. In between the plates, a layer of glass

wool (100 mm thick) was inserted to provide thermal insulation. The test section dimensions are illustrated in Figure 3. Screens are employed to provide a uniform air flow in the inlet and outlet sections and also upstream of the air flow nozzles. In this region, the height of the test section was increased to accommodate the nozzle array used for measuring the air flow rate.

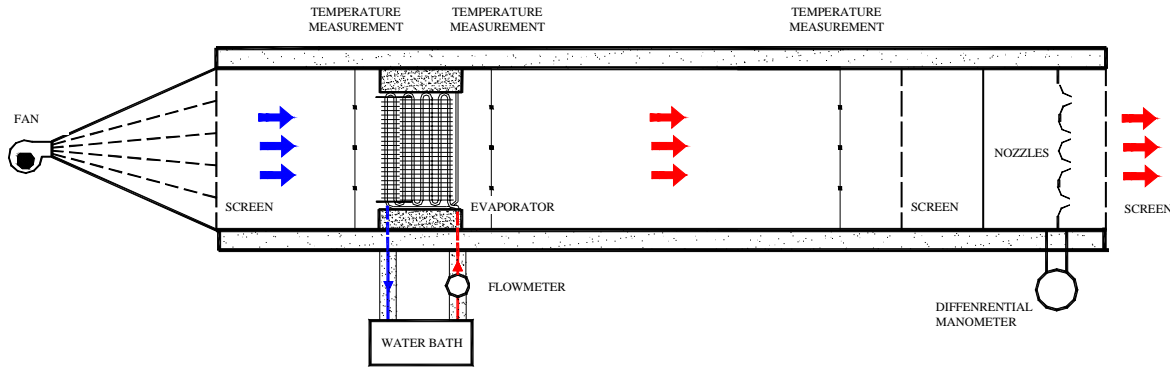


Figure 3. Schematic representation of the experimental apparatus.

The wind tunnel air-side instrumentation is as follows: a 51-W speed controlled fan (EBMPapst, G1G144-AE13-50), a 400-W (max.) PID controlled electrical resistance for air inlet temperature setting, a set of 5 aluminium nozzles (Helander Metal) with diameters ranging from 0.75" to 1.25", and 2 differential pressure transducers (DRUCK LXP1010 and LXP1510) to measure the air pressure drop across the evaporator and the nozzles. The evaporator pressure drop is measured by placing perforated hoses (holes 50 mm apart) upstream and downstream of the evaporator. One end of each hose is connected to the pressure transducer while the other remains sealed. The accuracy of each pressure transducer is $\pm 0.5\%$ of the full scale (the full scale is ~ 25 Pa for the evaporator transducer and ~ 995 Pa for the nozzle transducer). Operation limits and design conditions are as follows, air flow rate: min $17 \text{ m}^3/\text{h}$ (10 cfm), max $102 \text{ m}^3/\text{h}$ (60 cfm), nominal $51 \text{ m}^3/\text{h}$ (30 cfm); heat transfer rate: min 15 W, max 200 W, nominal 120 W. Maximum evaporator dimensions are: height 250 mm, length 580 mm, width 80 mm.

A water loop was built to provide hot water for circulation inside the tubes at controlled temperatures and flow rates through the evaporator. The following components make the water circuit: a 1.58 L/min (max.) speed-controlled rotary pump (Procon 113E025F31BC100), a 100°C (max.) $\pm 0.1^\circ\text{C}$ accuracy, thermostatic bath (Microquímica), and a 1.89 L/min (max.), 1.4% full scale accuracy, turbine flow meter (Sponsler, MF80-CS). The loop is thermally insulated and type-T immersion thermocouples ($\pm 0.1^\circ\text{C}$ accuracy) are placed immediately upstream and downstream of the evaporator. Data acquisition is performed with a PC integrated 40 channel system (Agilent/HP, 34980A). This system, in conjunction with a purpose-built control panel, monitors and records pressure, temperature, relative humidity and water flow rate signals.

2.3. Experimental Procedure

The apparatus is switched on and the inlet water temperature (approximately 31 to 33°C in all cases) is set on the thermostatic bath and approximately 10 minutes are required for it to stabilize. The desired air flow rate is adjusted and the inlet air temperature is set (approximately 28 to 29°C in all cases). The water flow rate is set so that a 4.0°C difference between the inlet and outlet water temperatures is observed. Approximately 50 to 80 minutes – depending on the values of air and water flow rates – are required to reach steady-state. The heat transfer rate (capacity) calculated based on the air and water streams (Eqs. 1 and 2) are compared and a relative deviation of less than 5% between them guarantees the correctness of the measurement of heat transfer rate on the air-side (absence of leakages etc.).

$$\dot{Q}_w = \dot{m}_w C_{p,w} (T_{w,i} - T_{w,o}) \quad (1)$$

$$\dot{Q}_a = \dot{m}_a C_{p,a} (T_{a,o} - T_{a,i}) \quad (2)$$

The water flow rate is subsequently increased so as to provide a 0.5°C or so difference between the inlet and outlet water temperatures. At this condition, the water behaves as an infinite capacity stream (approximately constant temperature) and the heat exchanger acts as closely as possible to an evaporator (where the refrigerant temperature in the tubes is nearly constant because of refrigerant phase change). Because of the small inlet to outlet water temperature

difference and the large uncertainties which may result from calculating the heat transfer capacity of the heat exchanger based on this difference, only the air-side heat transfer rate (Eq. 2) is used in the data processing.

In all experimental runs conducted in this work, after steady-state had been reached (according to the criterion developed and tested by Hermes, 2006), temperature, pressure and mass flow rate signals were recorded and averaged over a time interval of 30 minutes. After data collection, the flow rates were altered and the procedure was repeated to achieve a new experimental condition.

2.4. Data analysis

The overall thermal conductance, UA , is calculated using the Log-Mean Temperature Difference approach with a true counterflow correction factor F assumed equal to unity because of the small water temperature difference,

$$UA = \frac{\dot{Q}_a \ln[(T_w - T_{a,in})/(T_w - T_{a,out})]}{(T_w - T_{a,in}) - (T_w - T_{a,out})} \quad (3)$$

where T_w is the arithmetic average between the inlet and outlet water temperatures. The air-side pressure drop was obtained directly from the evaporator differential pressure transducer measurement by subtracting the localized pressure drops due to contraction and expansion from the differential pressure measurement as follows,

$$\Delta p = p_{in} - p_{out} = \Delta p_{PT} + \Delta p_C + \Delta p_E \quad (4)$$

where the subscripts PT , C and E refer to pressure transducer, contraction and expansion, respectively.

An uncertainty analysis of the air flow rate, heat transfer rate and overall thermal conductance was carried out. The uncertainty associated with each parameter was estimated through (INMETRO, 2003),

$$u(Y) = k_f u_c(Y) \quad (5)$$

where k_f and $u_c(Y)$ represent the coverage factor and the combined standard uncertainty, respectively. k_f was assumed equal to 2, which corresponds to 95% of coverage probability. The air flow rate, the heat transfer rate and the overall thermal conductance can be written in a general form as Eq. (6), where $u_c(Y)$ is obtained through the error propagation law (Eq. 7),

$$Y = \bar{y} = \frac{1}{k} \sum_{j=1}^k y(X_{1,j}, X_{2,j}, X_{3,j}, \dots, X_{N,j}) \quad (6)$$

$$u_c(Y) = \sqrt{\sum_{i=1}^N \left(\frac{\partial Y}{\partial X_i} u(X_i) \right)^2} \quad (7)$$

where X_i is the i^{th} of N measured variables, $u(X_i)$ is the uncertainty related with these variables and k is the number of measurements undertaken to determine y . For calculating the air flow, the following parameters were measured: differential pressure across the nozzles, nozzle area and air flow temperature and pressure. The maximum uncertainties corresponding to the air flow rate, heat transfer rate and overall thermal conductance were $\pm 1.48\%$, $\pm 3.60\%$ and $\pm 3.89\%$, respectively.

3. COMPUTATIONAL FLUID DYNAMICS (CFD) MODELING

In order to assess the prediction capabilities of CFD simulations in 'no-frost' evaporator design, a numerical model of the air-side flow through evaporators #1 and #3 was implemented using the commercial code FLUENT 6.3 (Fluent, 2006). In this package, numerical solution of mass, momentum, energy, turbulent kinetic energy and turbulent dissipation rate was carried out using the Finite Volume Method. General-form conservation equations are as follows

$$\frac{\partial}{\partial t}(\rho\Phi) + \nabla \cdot (\rho\vec{v}\Phi - \Psi\nabla\Phi) = S_\Phi \quad (8)$$

where the diffusion coefficients and source terms associated with each conserved property are available in Versteeg and Malalasekera (1995). The two-equation k - ε realizable turbulence model of Shih *et al.* (1995) was utilized in conjunction

with the enhanced wall treatment scheme. This scheme deactivates wall functions in areas where grid resolution is fine enough to resolve the viscous sublayer. Because of the high thermal conductivity and small thickness of the fins, the FLUENT Shell Conduction Model was adopted to calculate the temperature field in these regions. The advantage of this scheme is that discretization of the solid regions is not needed.

The 3D computational meshes for evaporators #1 and #3 are shown in Figs. 4.a and b. The numbers of grid points are 266,976 and 199,536 for evaporators #1 and #3, respectively. Zones of flow development upstream and downstream of the evaporator were inserted in the computational domain for improving convergence. The problem geometry was set so that the fin lies on the mid-plane of the symmetric unit cells shown in Fig. 4. Periodic boundary conditions were specified on the centre planes of the air side channels. Uniform velocity and temperature were specified at the inlet of the computational domain and a pressure boundary was specified at the outlet section. The flow was assumed steady and incompressible. Thermophysical properties of air and aluminium were assumed constant at 29°C. Thermal contact resistances between fins and tubes, viscous dissipation and radiation effects were neglected. Turbulence intensities of 10% were specified at the evaporator inlet and outlet. The surface temperature of the tubes was assumed constant and calculated based on the arithmetic average between the inlet and outlet water temperatures of each experimental test. This value was then corrected to take into account the conduction thermal resistance of the tube walls.

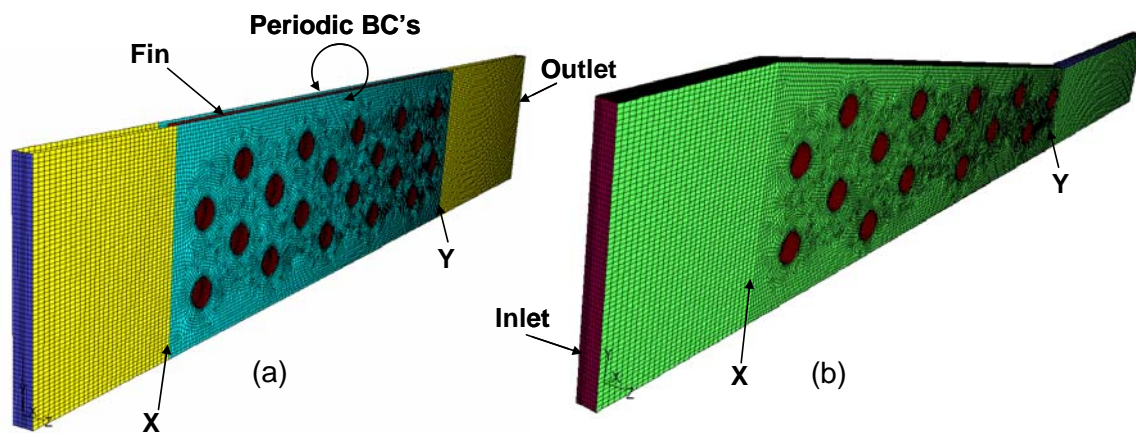


Figure 4. Computational mesh for elementary cell of the CFD simulation of evaporators #1 and #3.

The power-law differencing scheme and the SIMPLEC pressure-velocity coupling algorithm (Versteeg and Malalasekera, 1995) were adopted in the numerical solution. The convergence criterion was set to 10^{-4} and the computational cost for each test case was approximately 40 CPU minutes on a Pentium 2GHz PC.

The air-side pressure drop across was calculated as the difference between cross-section area-averaged static pressures on planes *X* and *Y* in Figs. 4.a and b. The heat transfer capacity of the unit cell was calculated from an integration of the local wall heat flux as follows,

$$\dot{Q}_C = \int_A -k_a \frac{dT_a}{dn} \Big|_{wall} dA \quad (9)$$

and the overall heat transfer capacity is calculated multiplying \dot{Q}_C by the number of elementary cells in the evaporator.

4. RESULTS AND DISCUSSIONS

4.1. Experimental Results

Table 1 shows the experimental results for the whole series of tests conducted in the present study. In total, 19 experimental runs have been conducted for the 4 evaporator samples. As can be seen, evaporator #1 presents the highest *UA* at all air flow rates. The overall thermal conductance ratio, defined by Eq. (10), as a function of air flow for the four samples is presented in Figure 5.

$$UA_{ratio,i} = \frac{UA_{\#i}}{UA_{\#1}}, \quad i = 2,3,4 \quad (10)$$

Although none of the AFEs tested here performed better than the baseline sample (evaporator #1), the experimental results for evaporator #3 demonstrate that even with 25% less heat transfer area, the magnitude of $UA_{\#3}$ is within approximately 15% of $UA_{\#1}$. This shows that, in theory, it may be possible to attain the same performance of sample #1 with an AFE of smaller heat transfer area. Furthermore, the results for evaporator #4 indicate that the way forward to increasing the UA of the AFE is not by means of further reducing the air-side flow cross-section in hope of obtaining a stronger increase in the local air-side heat transfer coefficient. In the case of sample #4, a little outlet height gives rise to an excessive reduction of the heat transfer area and the progressively higher air-side local Reynolds number (due to acceleration) is not enough to generate an overall thermal conductance compatible with that of the baseline case. On the other hand, by comparing the overall thermal conductance ratio of samples #2 and #3, one confirms the greater importance of the total number of fins on UA for a fixed outlet height. Thus, for a given fin pitch, one should expect that the overall thermal conductance ratio will reach an optimum at an outlet height larger than one-half of the inlet height. In addition, it should be mentioned that the overall material cost of the heat exchanger is not related to the volume of aluminium in a straightforward way. Since the fins are less expensive than the tubes, the cost of the AFE is expected to be less because the overall tube length is lower than in the baseline configuration.

Table 1 – Summary of test conditions.

Sample N°	Air Flow Rate (m ³ /h)	T _{a,in} (°C)	T _{a,out} (°C)	Water Flow Rate (m ³ /h)	T _{w,in} (°C)	T _{w,out} (°C)	ΔT _{lm} (°C)	Q _a (W)	Δp (Pa)	UA (W/K)
#1	34.78	28.15	29.73	0.042	31.04	30.46	1.682	18.02	2.44	10.71
	51.09	28.17	29.76	0.073	31.09	30.65	1.783	26.64	5.23	14.94
	67.96	28.24	29.78	0.068	31.04	30.49	1.637	34.68	7.68	21.18
	85.13	28.16	29.65	0.074	31.06	30.44	1.745	41.66	11.33	23.87
	103.45	28.22	29.60	0.084	31.00	30.40	1.702	46.46	16.08	27.30
#2	34.49	29.84	31.05	0.036	32.88	32.39	2.134	13.57	2.65	6.36
	51.25	29.82	31.08	0.046	32.88	32.37	2.108	20.96	6.36	9.94
	68.26	29.86	31.04	0.054	32.86	32.35	2.104	26.23	11.40	12.47
	85.35	29.85	30.96	0.063	32.86	32.35	2.148	30.84	17.64	14.36
	102.52	29.84	30.88	0.071	32.90	32.39	2.245	34.80	25.38	15.51
#3	34.40	29.80	31.33	0.045	32.93	32.40	2.003	17.12	5.68	8.55
	51.59	29.82	31.41	0.058	32.94	32.40	1.952	26.49	11.53	13.57
	68.53	29.84	31.40	0.076	32.90	32.40	1.925	34.73	19.49	18.04
	85.56	29.85	31.36	0.087	32.94	32.43	1.987	42.22	27.79	21.25
	102.48	29.83	31.32	0.099	33.00	32.48	2.076	49.66	35.87	23.92
#4	34.42	28.21	29.13	0.036	31.05	30.50	2.069	10.39	10.33	5.03
	50.97	28.23	29.29	0.057	31.04	30.57	2.001	17.64	19.63	8.82
	68.52	28.24	29.30	0.058	31.05	30.51	1.964	23.89	32.62	12.17
	90.63	28.24	29.35	0.082	31.08	30.59	1.983	32.92	52.49	16.60

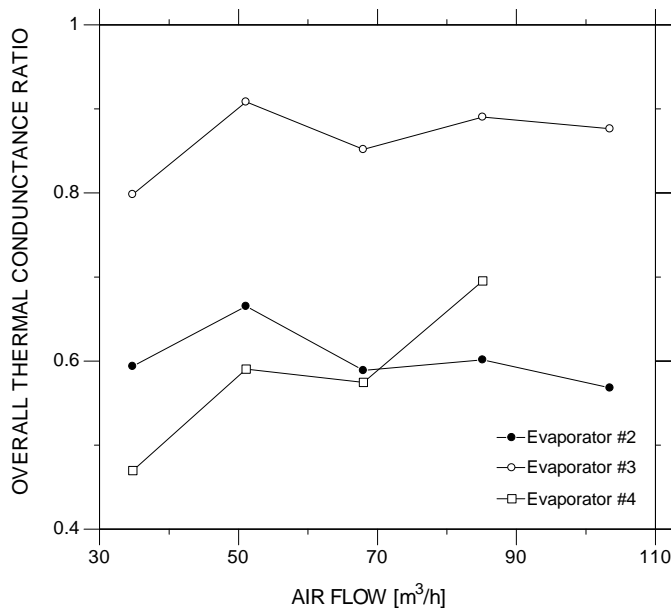


Figure 5. Overall thermal conductance ratio.

Figure 6 presents the overall heat transfer coefficient, U , of each evaporator as a function of the air flow rate. This was calculated as the ratio of UA (determined experimentally) and the overall heat transfer area of fins and tubes. The overall trend of U as a function of air flow rate for evaporators #1, #2 and #3 is analogous (concave curves) and the combined effect of flow acceleration and larger fin spacing increases the air-side thermal conductance in evaporator #2 with respect to samples #1 and #3. Surely as a result of flow acceleration, the overall heat transfer coefficient of evaporator #4 exhibits a linear (almost convex-shaped) behaviour with respect to the air flow rate. From Figs. 5 and 6 it can be concluded that the acceleration effect of evaporator #4 may be beneficial in terms of heat transfer enhancement only at air flow rates much higher than those normally encountered in household refrigerators (and hence beyond the range of the present experiments).

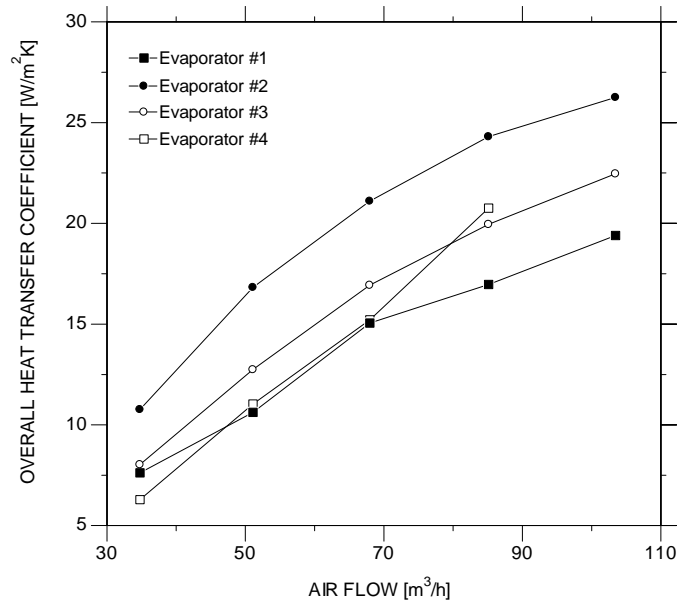


Figure 6. Air-side overall heat transfer coefficient.

Figure 7 presents the air-side pressure drop ratio as a function of air flow rate. The pressure drop ratio is defined as follows

$$\Delta p_{ratio,i} = \frac{\Delta p_{\#i}}{\Delta p_{\#1}}, \quad i = 2,3,4 \quad (11)$$

where the localized pressure drop due to contraction and expansion at the inlet and outlet of the air-side channel have been subtracted from the experimental pressure drop in all evaporators. As can be seen, the pressure drop in all AFEs is higher than in the baseline sample (evaporator #1). Moreover, pressure drop seems to be more sensible to the effect of smaller outlet height (i.e., air flow acceleration) than the overall thermal conductance. As expected, for a fixed outlet height, the number of fins increases the air flow pressure drop.

In Fig. 8, only the pressure drop due to friction, $\Delta p_{f\#i}$, (i.e., the irreversible part of the total pressure drop) has been normalized with respect to $\Delta p_{\#1}$. The frictional pressure drop was obtained combining the mass and momentum conservation equations to calculate the total pressure drop across an increment of length dz as follows

$$-dp = dp_f - \frac{\dot{M}^2}{\rho A_C^3} dA_C \quad (12)$$

where dp_f is the frictional pressure drop, ρ is the average air density, A_C is the cross-section area and \dot{M} is the mass flow rate. As $A_C = WH$ and

$$\frac{d}{dz} A_C = W \frac{dH}{dz} = -W \frac{H_{in} - H_{out}}{L} = -W \tan \theta \quad (13)$$

substituting Eq. (13) into Eq. (12) and integrating from $z = 0$ to L , one has

$$\Delta p_f = p_{in} - p_{out} - \frac{\dot{M}^2 \tan \theta}{\rho W^2} \frac{L(2H_{in} - L \tan \theta)}{2H_{in}^2 (H_{in} - L \tan \theta)^2} \quad (14)$$

The effect of acceleration on pressure drop was only significant for evaporator #4, where it accounts for as much as 20% of the pressure drop between provides is shown as a function of air flow rate.

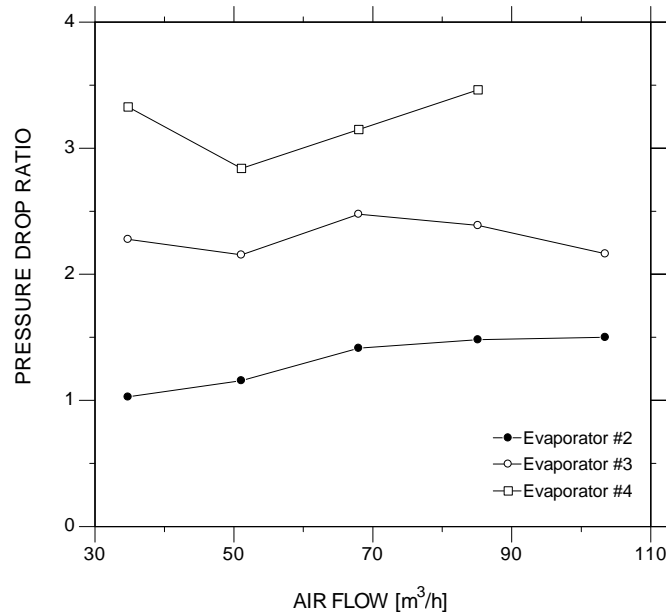


Figure 7. Air-side pressure drop ratio.

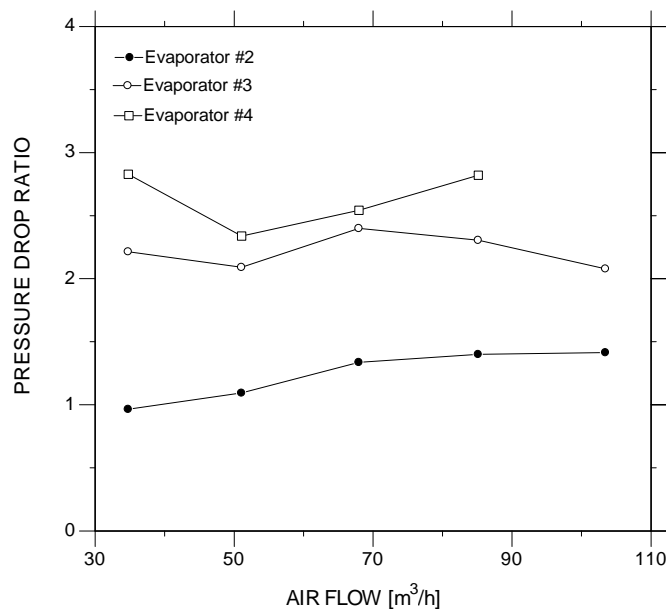


Figure 8. Air-side pressure drop ratio without the influence of acceleration.

4.2. CFD Simulation

Figures 9 to 11 present fin temperature, (mid-plane) air temperature and (mid-plane) air velocity distributions for an air volume flow rate of 68 m³/h (evaporator #1) and 68.5 m³/h (evaporator #3), respectively. These conditions correspond to face velocities of approximately 1 m/s for evaporators #1 and #3. The temperature distribution in the fins is approximately uniform in both cases, except for the upper left-hand corner where there is a region far from any tube

in contact with the cool air. Most certainly, the fin efficiency will not be so high in real applications where contact resistances exist due to discontinuities between fins and tubes.

The flow by-pass through the gaps between the tube bank and the top and bottom walls is clearly seen in the flow velocity distributions of Fig. 10. The by-pass is a result of the higher pressure drop resistance of the tube bank in comparison with that of the gaps. For a total flow rate of approximately 68 m³/h, the CFD calculations of evaporator #1 show that 29.8% and 29.2% of the total air flow rate by-passes the tube bank through the top and bottom gaps, respectively. At the same total flow rate, for evaporator #3, the by-pass fractions through the top and bottom gaps are 22.4% and 31.8%. Since the by-pass results in velocity and temperature stratifications on the air-side (see Fig. 11), this has a negative impact on the temperature effectiveness of the heat exchangers and should be minimized at all costs.

In real applications, the flow by-pass is minimized due to the presence of aluminium sheathed electrical heaters placed in the side gaps alongside the tubes. The heaters are switched on periodically and their main function is to melt the accumulated frost (by Joule-effect), thus avoiding blockage of the air-side passages which results in high air-side pressure drop and high transfer resistance.

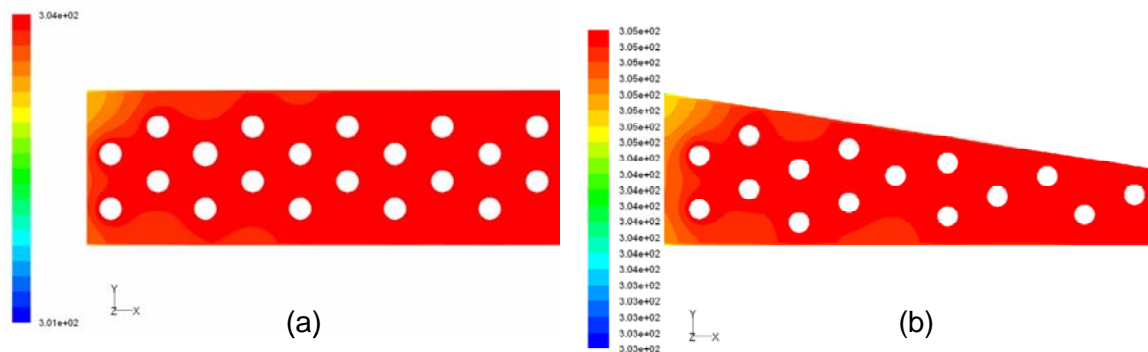


Figure 9. Fin temperature (scale in K) distributions.

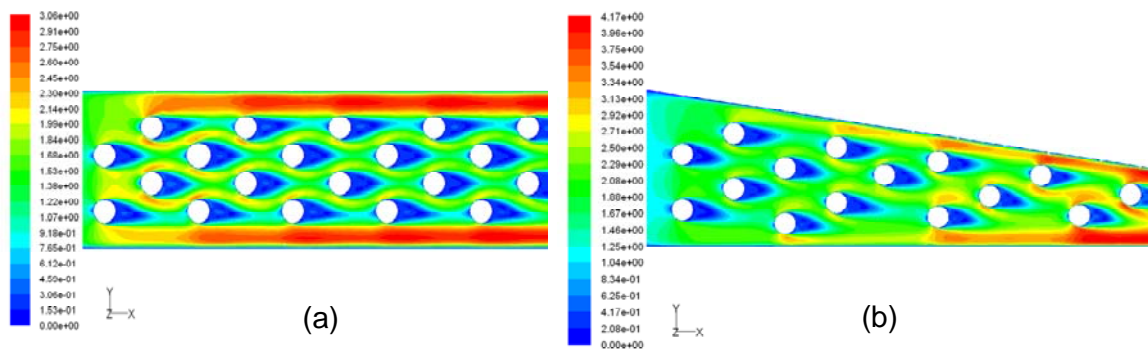


Figure 10. Flow velocity (scale in m/s) distributions (mid-plane).

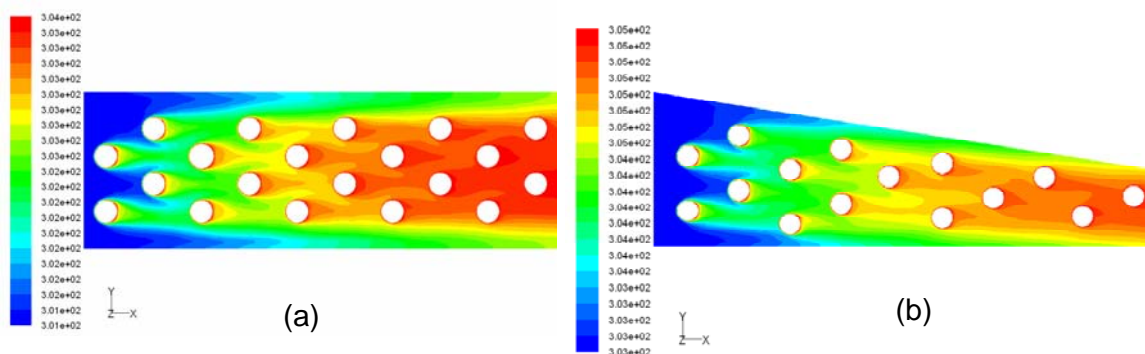


Figure 11. Flow temperature (scale in K) distributions (mid-plane).

Figure 12 shows a comparison between the experimental and calculated overall heat transfer capacity and total pressure drop for evaporators #1 and #3, respectively. Although the pressure drop is quite well predicted by the CFD

simulations, the calculated heat transfer capacity (not shown here) overpredicted the experimental results by more than 50%. Currently, refinements in the CFD analysis are being sought in order to improve the heat transfer prediction of the experimental data.

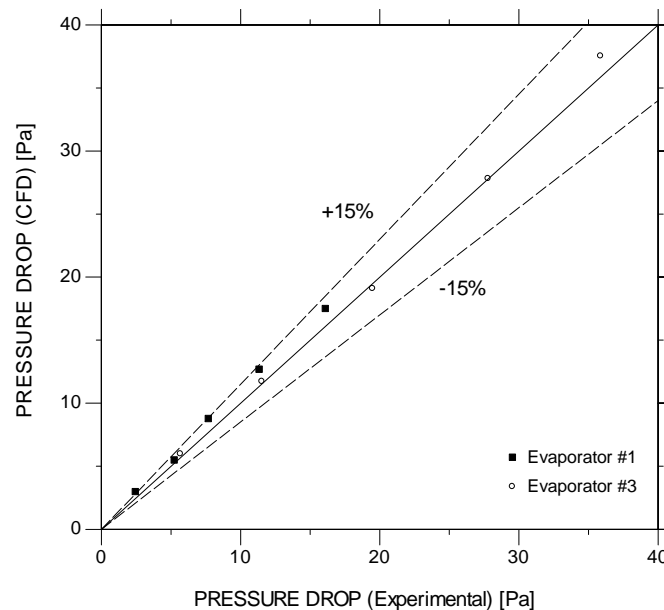


Figure 12. Comparison between the experimental and CFD pressure drop.

6. CONCLUSIONS

This paper presented experimental data on the thermal-hydraulic performance of a new concept of evaporator to be used in 'no-frost' household appliances. An open-loop wind-tunnel test facility especially designed and built for testing heat exchangers was utilized and data on heat transfer capacity, overall thermal conductance and pressure drop were collected for four samples with different geometric characteristics. The main conclusions arising from this study are as follows:

1. The experimental data provided an insight on the behaviour of the heat transfer enhancement and pressure drop in accelerated flow evaporators (AFE). The results serve as a starting point for future developments regarding optimization of geometrical parameters (e.g. number of fins, outlet height, etc.) for maximizing performance;
2. The experimental results showed that the AFE concept is capable of delivering a similar heat transfer performance as a standard (baseline) evaporator with less surface area and a lower number of tubes (i.e., less material cost). An intrinsic disadvantage of the AFE is that it presents a higher pressure drop. Nevertheless, in household appliances, the pressure drop due to the evaporator is generally small compared to that of the whole cold air delivery circuit in the refrigerator. Therefore, it could be easily accommodated by other components of the system.
3. A CFD model was implemented in a commercial package to obtain a numerical evaluation of the thermal-hydraulic performance of the AFE. Several aspects of the flow in 'no-frost' evaporators could be observed in the CFD simulations results such as flow by-pass and temperature maldistribution. Despite the overprediction of the heat transfer capacity, the agreement between the pressure drop prediction and experiments were satisfactory for evaporators #1 and #3. Validation of CFD modelling is of great importance for future studies with different heat exchanger configuration, enabling the generation of new results without the necessity of running new experiments for other configurations.

7. ACKNOWLEDGEMENTS

The authors are grateful to Israel Machado and Geovani Rodrigues for technical assistance. Financial support of Whirlpool Corporation and CNPq is duly acknowledged.

8. REFERENCES

ANSI/ASHRAE 37, 1988, *Methods of Testing for Rating Unitary Air-Conditioning and Heat Pump Equipment*.

- ANSI/ASHRAE 41.2, 1987 (RA 92), *Standard Methods for Laboratory Airflow Measurement*.
- ANSI/ASHRAE 51, 1999, *Laboratory Methods of Testing Fans for Aerodynamic Performance Rating*.
- Coulomb, D., 2006, "Refrigeration: The challenges associated with sustainable development", *Proceedings of the 6th International Conference on Compressors and Coolants, Slovak Republic*, CD-ROM.
- Cur, N. O. e Anselmino, J. J., 1992, "Evaporator for Home Refrigerator", *US Patent*, 5.157.941.
- FLUENT 6.3, 2006, User Manuals, Fluent Inc.
- Hermes, C. J. L., 2006, "A Methodology for Transient Simulation of Domestic Refrigerators" (in Portuguese), *D. Eng. Thesis*, Federal University of Santa Catarina.
- INMETRO, 2003, "Guide to the Expression of Uncertain in Measurement", Third Edition, ABNT, Rio de Janeiro.
- Karatas, H., Dirik, E., Derbentli, T., 2000, "An experimental study of air-side heat transfer and friction factor correlations on domestic refrigerator finned-tube evaporator coils", *Eighth International Refrigeration and Air Conditioning Conference at Purdue*, West Lafayette, Indiana – USA, July 25-28.
- Lee, T-H., Lee, J-S, Oh, S-Y, Lee, M-Y, 2002, "Comparison of air side heat transfer coefficients of several types of evaporators of household freezer/refrigerators", *Ninth International Refrigeration and Air Conditioning Conference at Purdue*, West Lafayette, Indiana – USA, July 16-19.
- Melo, C., Boeng, J., Piucco, R. O., 2004, *No-Frost Evaporators Thermal & Hydraulic Performance*, POLO/Multibrás, *Internal Report*, POLO Labs., Department of Mechanical Engineering, Federal University of Santa Catarina.
- Shih, T.-H., Liou, W.W., Shabbir, A., Yang, Z. and Zhu, J, 1995, "A New Eddy-Viscosity Model for High Reynolds Number Turbulent Flows - Model Development and Validation". *Computers and Fluids*, 24(3):227-238.
- Versteeg, H.K., Malalasekera, W., 1995, "An Introduction to Computational Fluid Dynamics: The Finite Volume Method", Pearson Prentice-Hall.